Effect of Stress Relieving Heat Treatment on the Microstructure and High-Temperature Compressive Deformation Behavior of Ti-6Al-4V Alloy Manufactured by Selective Laser Melting

YOUNG-KYUN KIM, SOON-HONG PARK, YONG-JIN KIM, BANDAR ALMANGOUR, and KEE-AHN LEE

This study aims to investigate the effect of stress relieving heat treatment on the microstructure and high-temperature compressive deformation behavior of the Ti-6Al-4V alloy, manufactured by selective laser melting. Initial microstructural observation confirmed elongated prior β grains in the building direction of both specimens (as-fabricated and heat-treated specimens). Along with such, the as-fabricated specimen only featured α'-martensite phase, while the heat-treated specimen featured α'-martensite and some α and β phases. Compression tests carried out at room temperature gave yield strengths of 1365 and 1138 MPa for the as-fabricated and heat-treated specimens, respectively. Such values are similar or greater than those of commercial wrought materials. The compressive fracture strain significantly increased after heat treatment. There was a general tendency of reducing yield strength as compressive temperatures increased. At temperatures greater than 700 °C, the as-fabricated and heat-treated specimens achieved similar strength. Microstructural observation after deformation confirmed that the initial microstructure was retained up to temperatures of 500 °C. At 700 °C or greater, both specimens showed drastic microstructural evolution.

I. INTRODUCTION

POWDER-BED additive manufacturing (AM) is an innovative technology that builds three-dimensional parts based on continuous powder layering based on a computer-aided design model.[1,2] Compared to conventional manufacturing processes (*e.g.*, casting, hot or cold working, or machining), the AM model has the advantage of fewer production stages and reduced material wastage. Complex parts are also processed easily with an increased flexibility of design.[3–5]

AM has more than one metal forming process. Selective laser melting (SLM) is the most widely used process. It is a powder bed fusion method where powdered metal is applied and a high-power laser is used for selective melting to manufacture complex and elaborate free-form parts.[6,7] When compared to other metal AM processes, such as direct energy deposition and e-beam melting, SLM is characterized by a relatively smaller layer thickness and fast cooling rate (10^5 to 10^8 K/s).[8,9] Due to such unique characteristics, SLM can manufacture parts with excellent dimensional accuracy and fine microstructure. The dislocation density increases during rapid solidification, resulting in increased hardness and strength.[10]

Among many alloys, Ti-6Al-4V (Ti64) alloy is one of the most commonly used materials in the Ti market and it has a variety of advantages such as outstanding specific strength, corrosion resistance, and bioaffinity.[11–13] With post–heat treatment of $\alpha + \beta$ phases, we can easily improve the microstructure, making it highly demanded by aerospace, medicine, and automotive industries and the military.[14–16] However, Ti64 alloy has high oxygen affinity, which requires particular control during the manufacturing processes and post-processing. Indeed, SLM can suppress oxidation and has excellent dimensional accuracy, making it ideal for manufacturing complex Ti64 alloy parts.

Due to the aforementioned advantage, various AM processes, including SLM, are used to manufacture Ti64 alloy, and multiple studies, including microstructure and

YOUNG-KYUN KIM and KEE-AHN LEE are with the Department of Materials Science and Engineering, Inha University, Incheon 22212, Republic of Korea. Contact email: keeahn@inha.ac.kr SOON-HONG PARK is with RIST, Pohang-si, Gyeongbuk 37673, Republic of Korea. YONG-JIN KIM is with KIMS, Changwon-si, Gyeongnam 51508, Republic of Korea. BANDAR ALMANGOUR is with the School of Engineering and Applied Sciences, Harvard University, Cambridge, MA.

mechanical properties, have been conducted to allow its application in various fields. In particular, microstructure control through process variables, process types, layering direction, and heat treatment[17–19] and various mechanical properties, including the tensile deformation of each building direction (BD), high-cycle fatigue, and fracture toughness, were reported.[20–22] Also, the authors recently reported heat treatment for improving high-temperature creep properties.[23] Indeed, it is commonly regarded that SLM Ti64 alloy forms full martensite structures due to its fast cooling rate. Such a martensite structure is highly brittle, which limits its application in many structural applications; therefore, heat treatment is beneficial in improving toughness and ductility. However, despite the previous studies, to the authors' knowledge, there is a lack of sufficient studies on the high-temperature deformation behavior of SLM parts.

The goal of this study is to investigate the influence of heat treatment on the microstructure and compressive properties of SLM Ti64 alloy. The study also aims at analyzing the deformed microstructure and surface after compression, which varies according to temperature to identify the high-temperature deformation/fracture mechanism of SLM Ti64 alloy.

II. EXPERIMENTAL METHOD

This study used Ti-6Al-4V (Ti64) manufactured by EOS. The specimen had BD, transverse direction (TD), and scanning direction (SD) sizes measuring 74.5, 12, and 7 mm, respectively. In addition, in the present study, a unidirectional scanning strategy was adopted. The chemical composition (wt pct) analysis of Ti64 alloy manufactured by SLM implemented using an X-ray fluorescence spectrometer (ZSX Primus II) confirmed Ti as well as 5.50Al, 3.87V, and 0.22Fe. Also, to identify the influence of stress-relieving heat treatment on the microstructure and mechanical property of the preceding materials, SLM Ti64 alloy was heat treated (stress relieving) in an Ar atmosphere at 650 °C for 3 hours and then cooled under furnace. The heating rate for the process was set at 10 °C/min.

To evaluate the room- and high-temperature compressive properties of SLM Ti64 alloy, a cylindrical compression sample in the BD direction was produced with a size of Φ 4-mm o.d. × 6-mm height. The compression tests were performed using MTS-810 equipment at room temperature, 500 °C, 700 °C, and 900 °C, and tests were conducted until total strain (ε_{tot}) = 0.6 with an initial strain rate 1×10^{-3}/s. The compression tests were conducted 3 times for each datum point. Hardness measurement was conducted using a Vickers hardness tester (Mitutoyo HV-100) at constant load 2 Kgf and holding time 10 seconds. A total of 12 measurements were made, and the average was calculated.

To analyze the phase transformations of SLM Ti64 alloy, an X-ray diffractometer (XRD, Ultima IV) was used. Further, to observe the microstructure before and after heat treatment, the specimens were cut at a vertical

angle in the TD and then mechanically polished using silicon carbide papers (#100 to #2000) and diamond suspension of 1 μm. The specimen was then etched in 50 mL H_2O + 25 mL HNO_3 + 5 mL HF solution before being observed using an optical microscope (OLYMPUS BX53M) and scanning electron microscopy (SEM, Tescan VEGA II LMU). Internal grain orientation and disorientation angle distribution were analyzed using electron backscatter diffraction (EBSD, Nordlys nano detector, binning: 4 × 4) analysis. The specimen was polished using silicon carbide paper and diamond suspension and was polished further with 0.01-μm colloidal silica before observation. EBSD observation was made at a step size of 100 nm and 15 kV, and the data obtained were analyzed using an imaging microscopy software (AZTecHKL) program. SEM and field-emission–SEM (Tescan MYRA 3 XMH) equipment were used to observe the compression specimen surface and microstructure after deformation, to identify deformation and fracture mechanisms according to temperature, after high-temperature compression.

III. RESULTS AND DISCUSSION

A. *Microstructures of SLM Ti-6Al-4V Alloys*

Figures 1(a) and (b) show macroscopic observations of microstructure before and after heat treatment, respectively, in the plane perpendicular to the TD; both specimens feature coarse columnar grains of approximately 50 to 100 μm in width along the BD. This observation occurred due to the unique characteristic of AM where heat is discharged during solidification in a single direction. While in conventional casting processes heat discharge is relatively even without a particular direction, SLM, in contrast, is known to discharge heat along the laser irradiation direction as the solid powder is melted.[24] As such, the structure of SLM Ti64 alloy develops in a single direction forming columnar grains and the structure observed is reported as prior β grain, which remains due to the fast cooling rate.[18] The microstructural differences between the two specimens were the elimination of dark bands, expected as the track line of the laser after heat treatment, and the decrease of the size and distribution of some defects. The density of the as-fabricated and heat-treated specimens, measured using Archimedes' principle, were 4.372 and 4.411 g/cm³, respectively, confirming that density increased after heat treatment.

Meanwhile, when the focus was shifted to the interior microstructure of columnar grains, fine acicular type structures were observed. These structures are suspected to be α'-martensite, and in general, Ti64 alloy, which has a low β-stabilizing element concentration, is known to form α'-martensite with a distorted hexagonal crystal lattice during rapid solidification.[25] In other words, it is suspected to be the result of the insufficient time for β phase into the stable $\alpha + \beta$ phase. Becker et al.[26] reported that the SLM process has a narrow layer thickness, which causes fast cooling rates, and this, in turn, results in the formation of fully martensite structures.
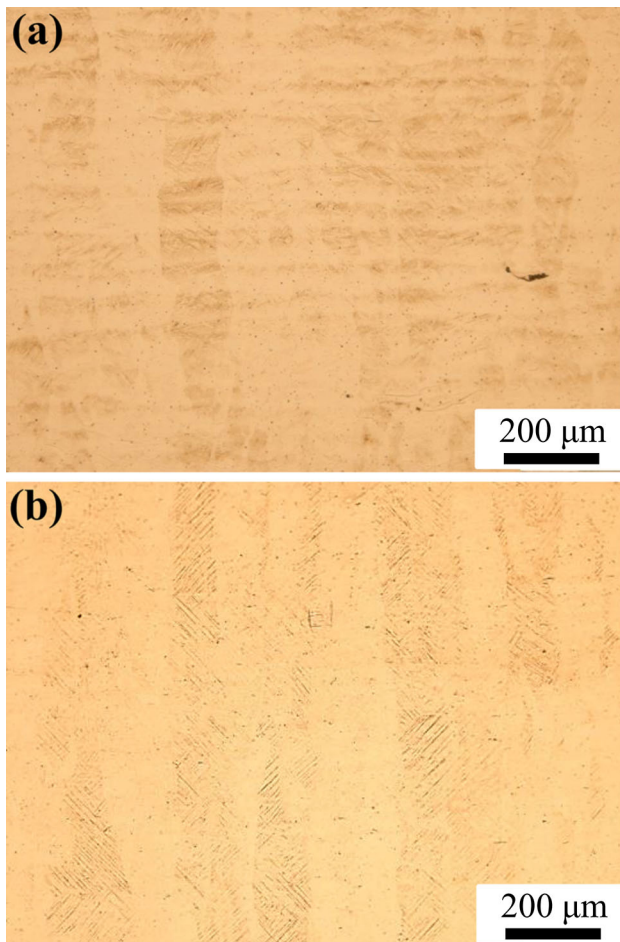
Fig. 1—Optical micrographs illustrating the wide columnar grains of the (a) as-fabricated specimen and (b) heat-treated specimen.
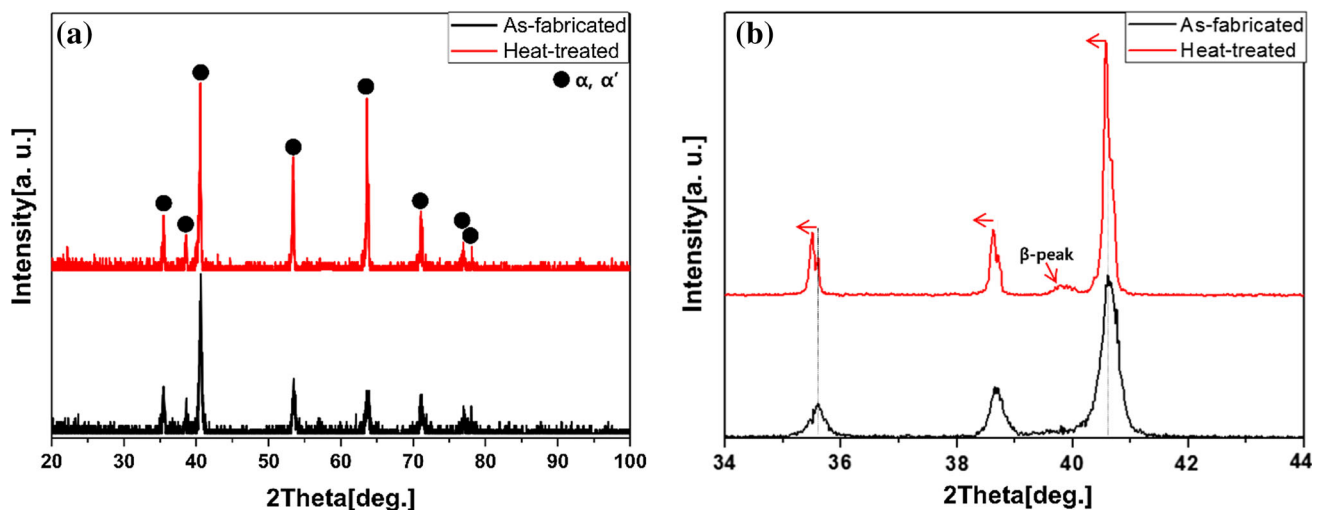
X-ray diffraction analysis results of the as-fabricated and heat-treated specimens are shown in Figure 2. When the peaks at 20 to 100 deg 2-theta were compared (Figure 2(a)), both specimens featured α or α′-martensite phase as their main phase and there were no significant differences between the two specimens. However, when the peaks were compared at 34 to 44 deg 2-theta with a slow scan rate (0.02 deg/min) (Figure 2(b)), some β peak was detected, while the peak of α or α′-martensite peak showed tendencies of shifting to lower 2-theta. This is commonly found when the martensite phase is decomposed into α phase. In other words, the material consists of α′ phase before heat treatment, and after heat treatment, the material consists of α′ phase along with some α and β phases.

Figure 3 is a high-magnification observation of the initial microstructure using SEM. As the XRD findings suggest, before heat treatment (Figure 3(a)), the specimen consisted dominantly of α′-martensite phase. The thickness of α′ measured approximately 0.1 to 1 μm. Meanwhile, the heat-treated specimen consisted of α′ phase along with α and β phases, and such a finding confirmed that α′ phase underwent phase decomposition during heat treatment.

The EBSD analysis was performed to identify the microstructural characteristics of the material mentioned previously in detail, and the findings are shown in Figure 4. First, the grain orientation map observation before and after heat treatment confirmed prior-β grain elongation and the columnar structures around the prior β-grain boundary were completely different. Also, a misorientation angle distribution analysis of the two specimens (Figure 5) shows dominant fractions of low-angle boundaries (LABs) at an angle less than 5 deg and high-angle boundaries (HABs) near 60 deg. This is assumed to be due to the unique characteristic of Ti and

Fig. 2—X-ray diffraction analysis results of an as-fabricated specimen and heat-treated specimen: (a) 20 to 100 2-theta and (b) 34 to 44 2-theta.
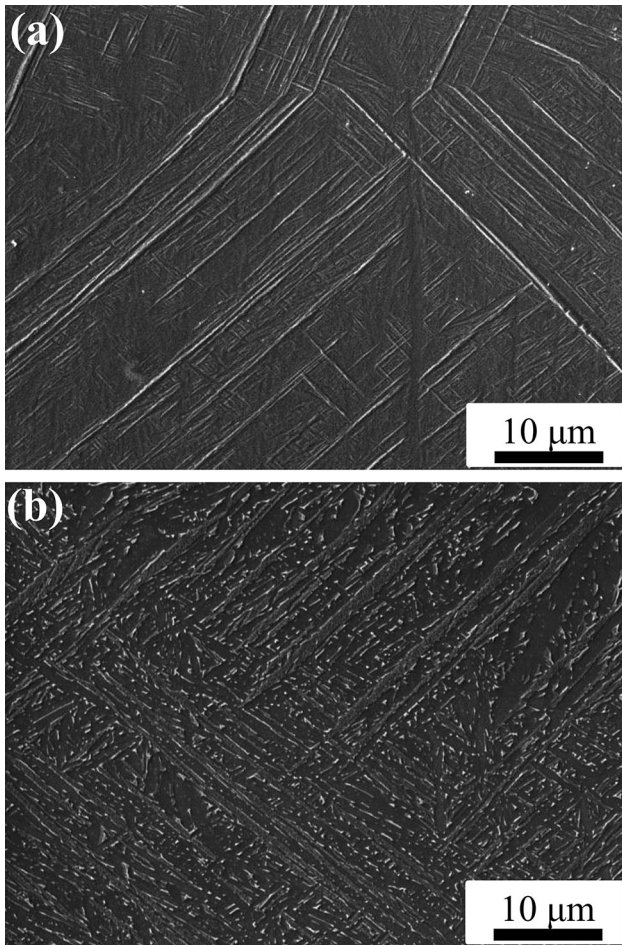
Fig. 3—SEM observation results after chemical etching showing the microstructures of (a) an as-fabricated specimen and (b) a heat-treated specimen.

Ti alloy during martensite structure formation where dislocation density drastically increases in the process of individual plane twinning. Simonelli et al.[27] reported that, generally, SLM Ti64 alloy has five to six α' planes within the prior β-grain, including $\langle 11\bar{2}0\rangle\alpha'$ with 60 deg orientation and martensite with 63.26 deg orientation. In other words, martensite can be formed by HABs around 60 deg, and it is assumed that dislocation density increases in this process through HABs, which also lead to an increase in LABs. Another point to note in the orientation angle distribution is the drastic decrease of the ratio of LABs after heat treatment.

In general, it is possible to calculate the geometrically necessary dislocation through the orientation difference near the point measured using EBSD and the continuum dislocation mechanics proposed by Nye and Kroner.[28–30] Thus, the geometrically necessary dislocation density distribution maps were analyzed and the results are shown in Figure 6. In the GND distribution maps, it can be seen that the as-fabricated specimen (a) has a relatively large amount of GNDs compared to the heat-treated specimen (b). In addition, the average GND densities were measured as $4.3 \times 10^{13}/\mathrm{m}^2$ and $2.2 \times 10^{13}/\mathrm{m}^2$ in the as-fabricated and heat-treated

specimens, respectively, and the GND density tended to decrease after heat treatment. In other words, the stress relieving heat treatment performed in this study was found to effectively reduce the internal dislocation density.

B. Room-Temperature Hardness Properties

Figure 7 shows the hardness measurement according to the direction of the as-fabricated and heat-treated specimens. In the case of the as-fabricated specimen, the hardnesses of planes perpendicular to the TD, SD, and BD measured 413 ± 6, 402 ± 7, and 448 ± 5 HV, respectively. Compared to planes perpendicular to the TD and SD, BD achieved approximately 10 pct higher hardness, indicating anisotropy in the mechanical properties. On the other hand, in the heat-treated specimen, the hardnesses of planes perpendicular to the TD, SD, and BD measured 369 ± 5 HV, 368 ± 5 HV, and 368 ± 3 HV, respectively, showing an overall decrease in average hardness and the removal of anisotropy in hardness. Hardness measured in this study was confirmed to be within the hardness range (352 to 521 HV) of previous SLM Ti64 alloy[31] studies. The decreased hardness is assumed to be due to the partial phase decomposition after heat treatment and lower dislocation density. Meanwhile, directional hardness measurement confirmed that heat treatment is an effective method to reduce the hardness anisotropy of SLM Ti64 alloy.

C. Room and High-Temperature Compressive Properties

Figure 8(a) shows the room- and high-temperature compressive results of the as-fabricated and heat-treated specimens. The room-temperature yield strengths before and after heat treatment measured 1365 ± 13 and 1138 ± 7 MPa, respectively, indicating a slight decrease in yield strength after heat treatment. Meanwhile, some fracturing occurred at a low strain ($\varepsilon_t \sim 0.1$) before heat treatment, but the fracture strain significantly increased ($\varepsilon_t \sim 0.35$) after heat treatment. The reason for the strength decrease and fracture strain increase is assumed to be the complex interaction between the decomposition of the brittle α' phase, which was confirmed in the XRD and SEM observation mentioned previously and the dislocation density decrease suspected from EBSD orientation angle distribution.

The room-temperature characteristics of the two specimens used in this study were compared to commercial cast and wrought materials[32] and the other SLM Ti64 alloys.[21,33,34] The as-fabricated and heat-treated specimens achieved 200 MPa or greater yield strength than cast materials and similar or slightly greater strength than wrought materials. The findings on SLM Ti64 alloy in this study were within the yield strength range previously reported. In particular, the as-fabricated specimen exhibited similar or greater yield strength compared to previous SLM materials. The SLM Ti64 alloy achieved greater strength due to the fast cooling rate that occurred during the melting and solidifying of initial solid powder. In other words, the
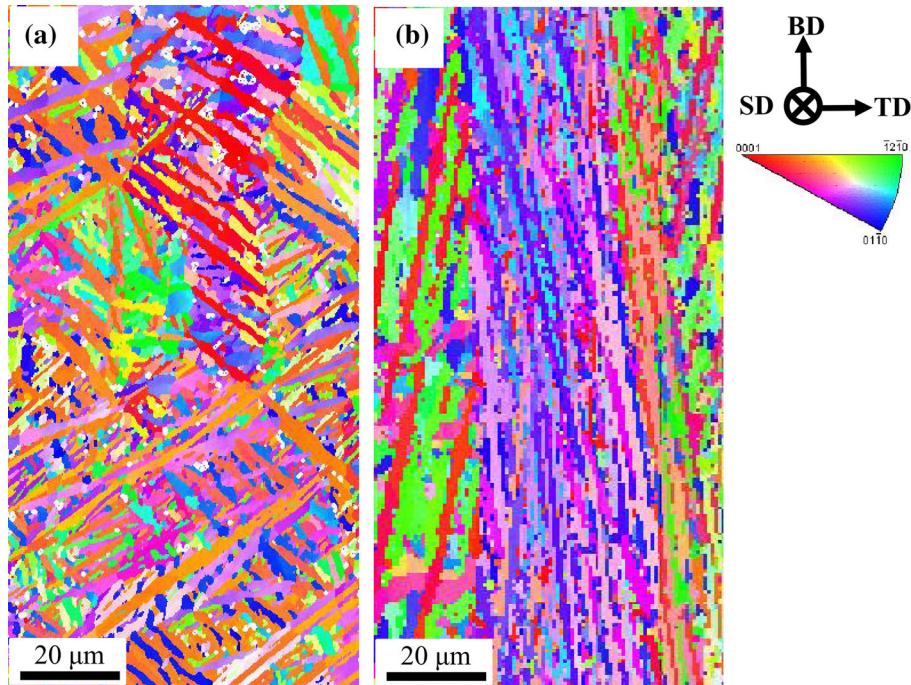
Fig. 4—EBSD grain orientation maps of SLM Ti-6Al-4V alloys: (*a*) as-fabricated specimen and (*b*) heat-treated specimen.

as-fabricated specimen formed fine martensite structures according to the aforementioned fast cooling rate (approximately 10^5 to 10^8 K/s)[8,9] that achieved greater strength.

The yield strength at various compression temperatures is shown in Figure 8(b). The yield strengths of the as-fabricated specimen tested at 500 °C, 700 °C, and 900 °C are 930 ± 9, 242 ± 8, and 45 ± 4 MPa and those of the heat-treated specimen are 600 ± 5, 246 ± 5, and 47 ± 3 MPa, respectively. The as-fabricated specimen achieved greater yield strength at room temperature up to 500 °C. However, in the 700 °C to 900 °C range, a drastic yield strength decrease occurred and the strength difference between the two specimens nearly disappeared. This drastic yield strength decrease at high temperature is assumed to be due to the extreme microstructural change around 700 °C. In general, the β recrystallization temperature of Ti-6Al-4V (manufactured by other conventional processes) is known to be approximately 800 °C to 850 °C, but there are incidents of dynamic recrystallization (DRX) occurring during high-temperature deformation (approximately 650 °C to 750 °C) reported.[35] Details of such shall be discussed along with the microstructural observation after deformation in Section III–D.

D. *Fracture and Compressive Deformation Behaviors*

The specimen surfaces were observed after room- and high-temperature compression tests, to identify the deformation/fracture behavior of the as-fabricated and heat-treated specimens; findings from the experiment are shown in Figure 9. Observation of room-temperature compression surfaces of the as-fabricated specimen
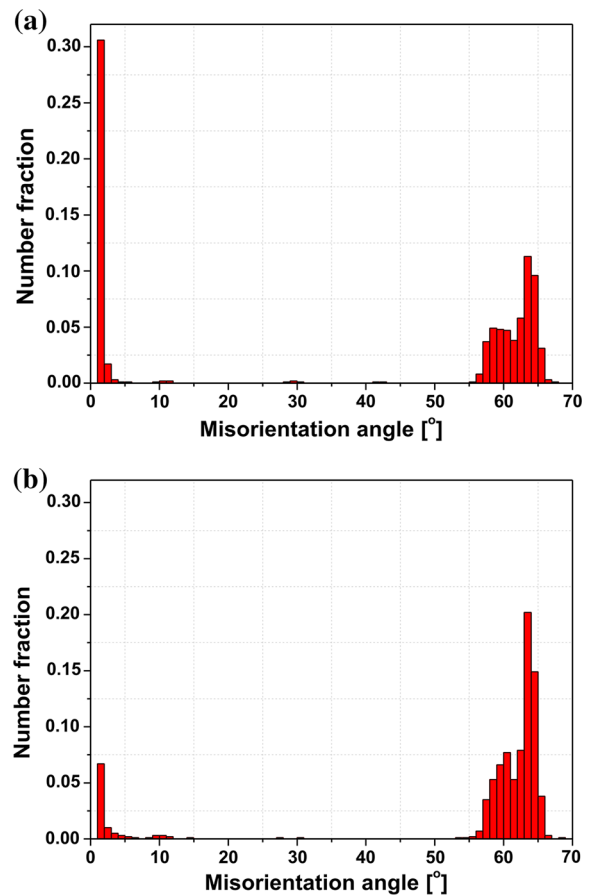

Fig. 5—EBSD misorientation angle distribution of SLM Ti-6Al-4V alloys: (*a*) as-fabricated specimen and (*b*) heat-treated specimen.
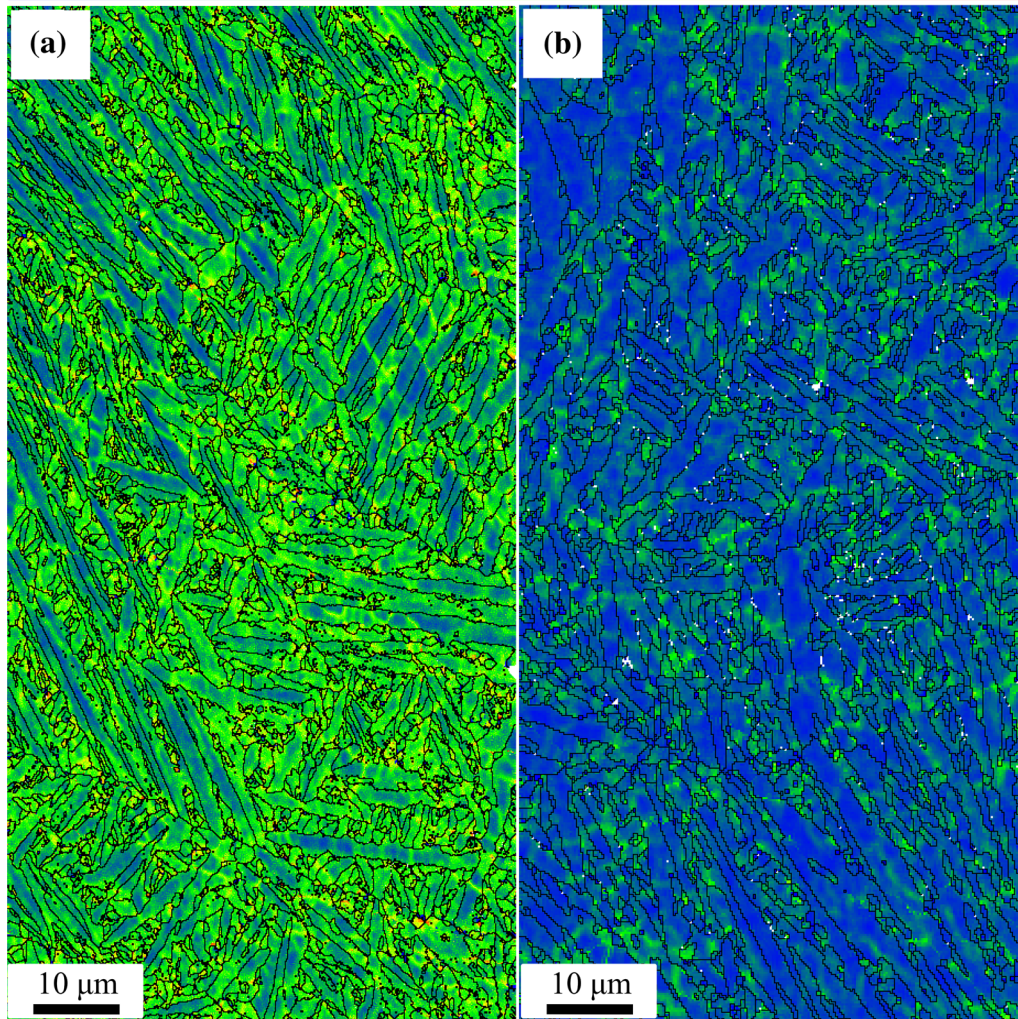
Fig. 6—EBSD geometrically necessary dislocation distribution maps of the SLM Ti-6Al-4V alloys: (*a*) as-fabricated specimen and (*b*) heat-treated specimen.

(Figure 9(a)) and heat-treated specimen (Figure 9(b)) confirmed a key difference in fracture behavior. In the as-fabricated specimen, there was nearly no morphological change ($\varepsilon_t \sim 0.1$) and there was a brittle fracture tendency in the 45 deg direction from the compression load application direction. On the other hand, the heat-treated specimen showed morphological change ($\varepsilon_t \sim 0.35$) due to deformation and only significant cracks were formed in the 45 deg direction without fracturing. In the observation of as-fabricated and heat-treated specimen surfaces after the 500 °C compression test, the as-fabricated sample showed relatively uneven deformation and some shear bands (or cracks) while the after-treatment specimen showed swelling of the specimen center according to a barreling effect without any further massive cracks. After the 700 °C compression test, surface oxidation was confirmed in both specimens regardless of heat treatment, and after the 900 °C

compression test, surface oxidation developed further in both specimens.

To further identify the surface characteristics of the findings mentioned previously, a high-magnification observation was conducted, as shown in Figure 10. In this case, the high-magnification observation was aimed at the specimen center where deformation was concentrated aside from the surfaces where massive cracks or fractures occurred. The as-fabricated specimen after the room-temperature compression test (Figure 10(a)) had well-developed shear bands unlike the brittle fracture tendencies observed in the low-magnification image. The heat-treated specimen (Figure 10(b)) also had well-developed shear bands. These shear bands are formed when deformation is concentrated in a localized region,[36] and generally, shear band formation can be considered as the evidence of deformation. In other words, while the macroscopic surface observation of the
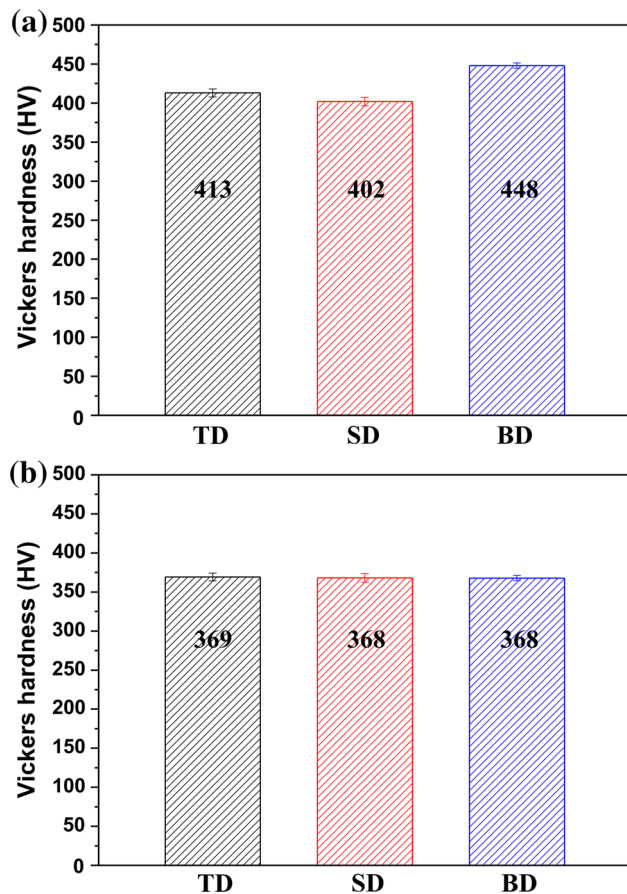
Fig. 7—Vickers hardness results of SLM Ti-6Al-4V alloys: (*a*) as-fabricated specimen and (*b*) heat-treated specimen.

Fig. 8—(*a*) True stress *vs* true strain compression curves and (*b*) yield strengths at various temperatures for a nominal strain rate of 10^{-3}/s.

as-fabricated specimen after the room-temperature compression test showed brittle fractures, microscopic observation showed ductile characteristics, such as shear band, indicating that partial deformation was accommodated. Meanwhile, high-magnification surface observation of the as-fabricated specimen after the 500 °C compression test confirmed massive cracks along the formation direction of shear bands. With such a finding, the massive cracks and fractures (500 °C and room temperature) are suspected to be related to shear band formation according to deformation concentration. On the other hand, high-magnification observation of the heat-treated specimen after the 500 °C compression test did not show any cracks. This is evidence that the heat-treated specimen achieved relatively ductile characteristics up to 500 °C compression conditions. In the case of specimens deformed at 700 °C, both specimens developed fine vertical cracks and surface oxidation was confirmed. After the 900 °C compression test, surface oxidation developed. Further, cracks became larger and vertical cracks developed unevenly.

However, in the room- and high-temperature compressive deformation behaviors of the preceding material, it is expected that the microstructure after deformation will have a greater influence than the surface characteristics. Thus, the microstructure after
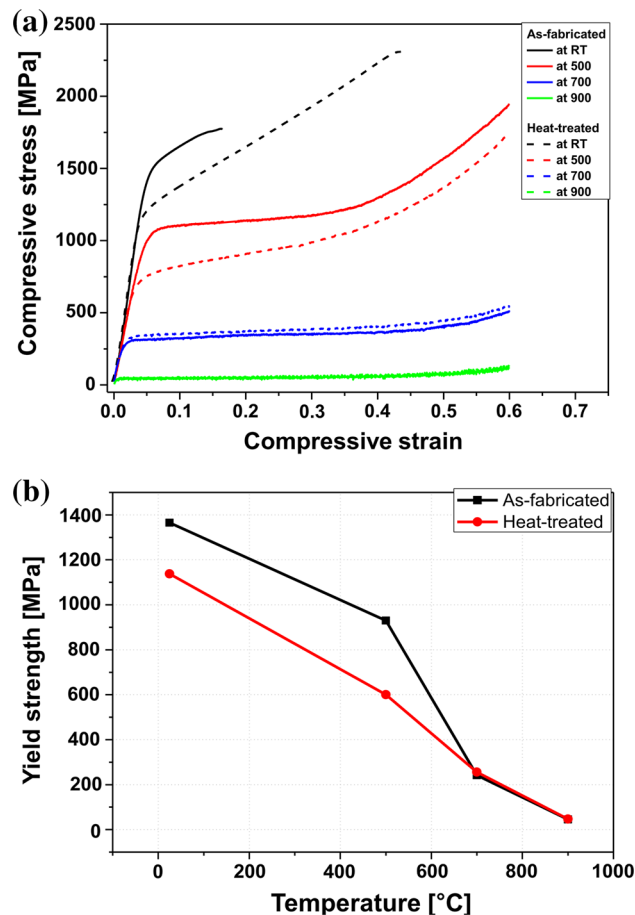
compressive deformation at 25 °C and 500 °C of the two materials was observed, and the results are shown in Figure 11. After the room-temperature compression test, the as-fabricated specimen (Figure 11(a)) showed a dominant martensite phase without significant differences compared to the initial microstructure. This is assumed to be due to deformation being concentrated in some regions and the plastic deformation not being accommodated. On the other hand, the deformation structure of the heat-treated specimen (Figure 11(b)) showed α′, α, and β phases coexisting, similar to the initial microstructure, and bending of martensite due to deformation was observed. In other words, the as-fabricated specimen had deformation concentrated in localized regions, causing brittle fracture tendencies without microstructural change, while the heat-treated specimen accommodated even deformation, resulting in the bending of the martensite plane and relatively ductile crack formation behaviors. Unlike the room-temperature condition, the 500 °C deformed microstructure of the as-fabricated specimen (Figure 11(c)) showed bending of some martensite planes, which is considered to be evidence of another deformation along with the morphological deformation found in the surface observation. When compared to the room-temperature
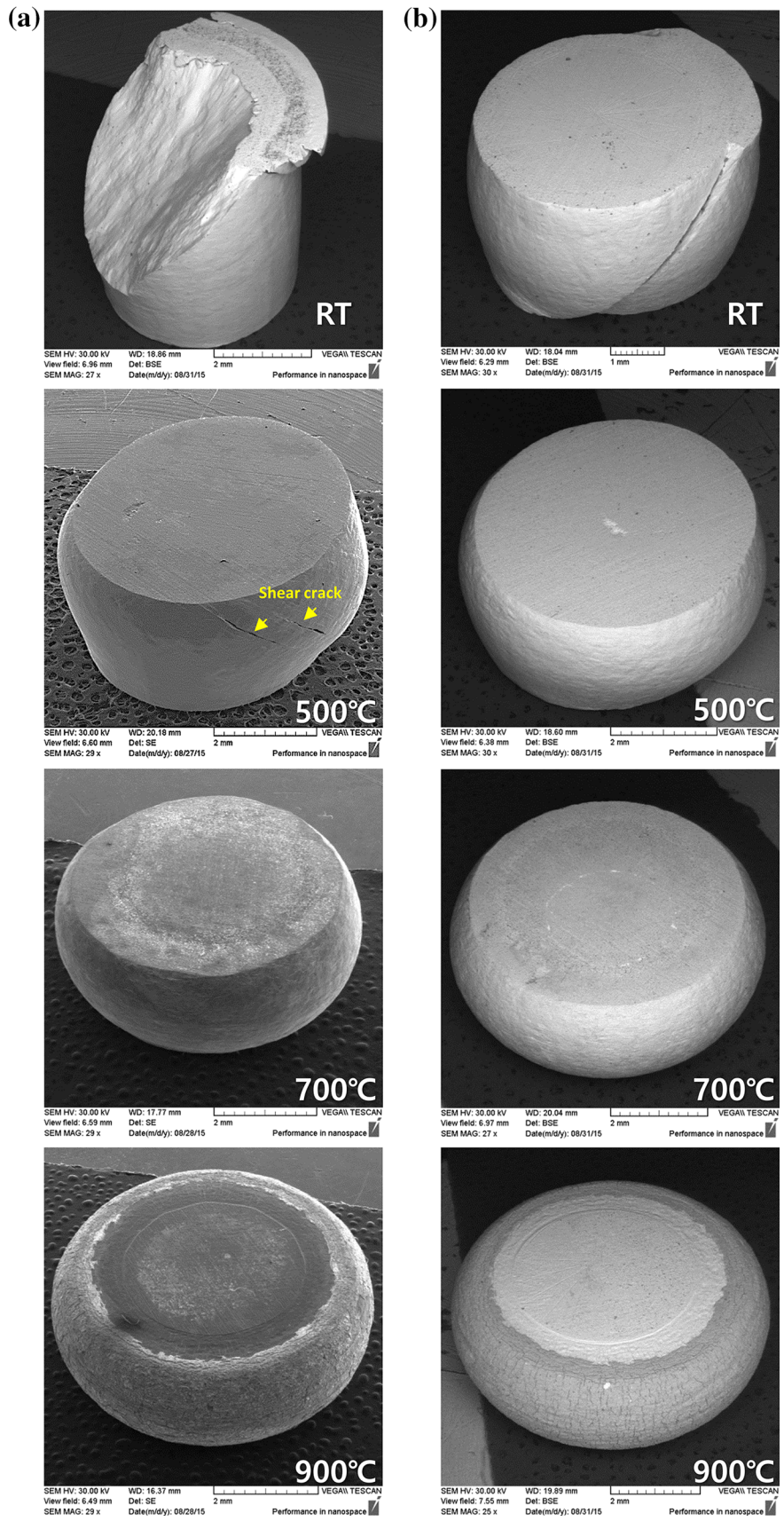
Fig. 9—Macrosurface images of (*a*) an as-fabricated specimen and (*b*) a heat-treated specimen after hot compression tests at various temperatures.
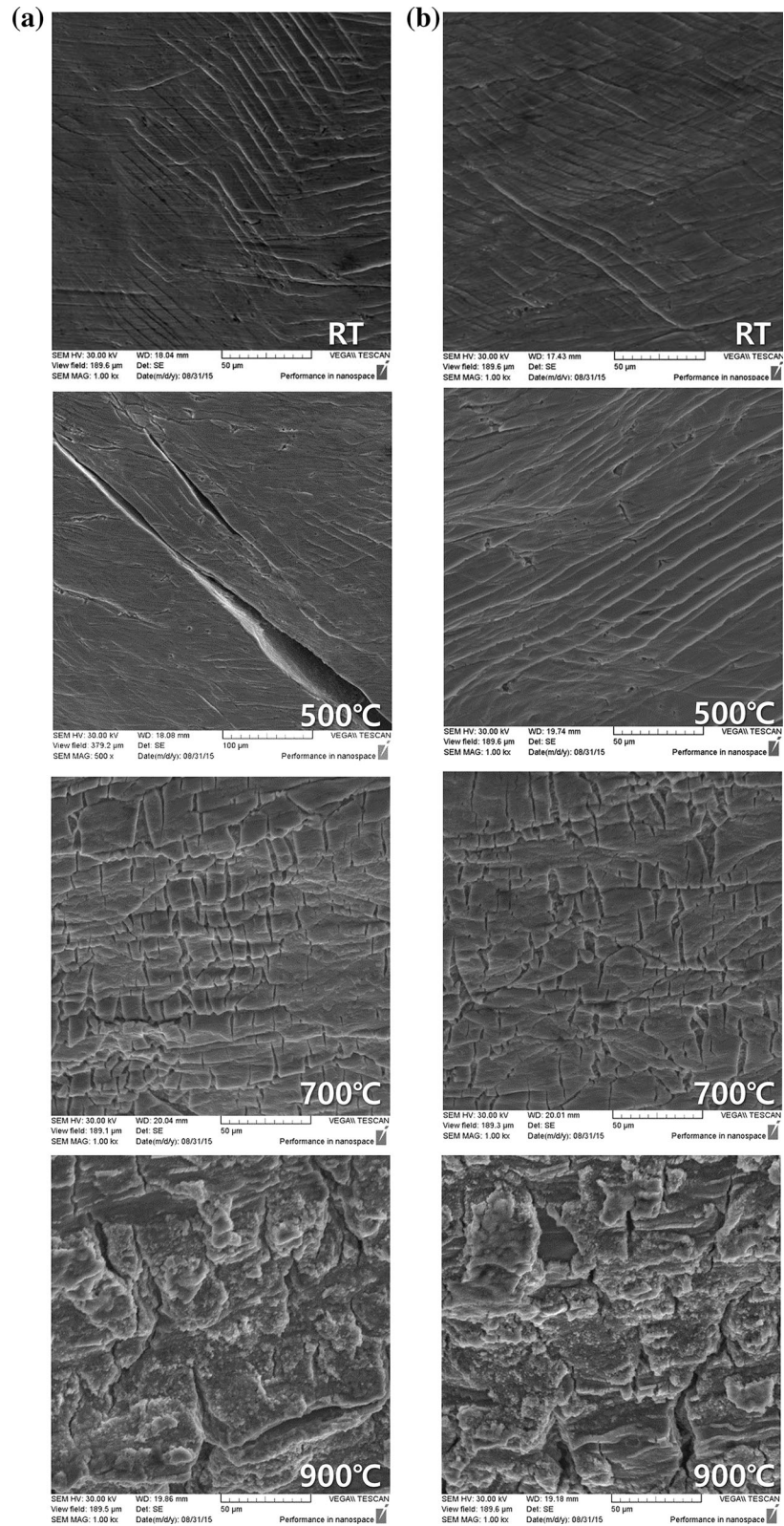
Fig. 10—SEM microimages of (*a*) an as-fabricated specimen and (*b*) a heat-treated specimen after hot compression tests at various temperatures.

compressive-deformed microstructure of the heat-treated specimen, the 500 °C compressive-deformed microstructure of the heat-treated specimen (Figure 11(d)) had α', α, and β phases coexisting, but

they featured microstructural characteristics that further accommodated the deformation (wavy martensite laths).

Figure 12 shows the microstructure after deformation at 700 °C or higher, where a difference in mechanical
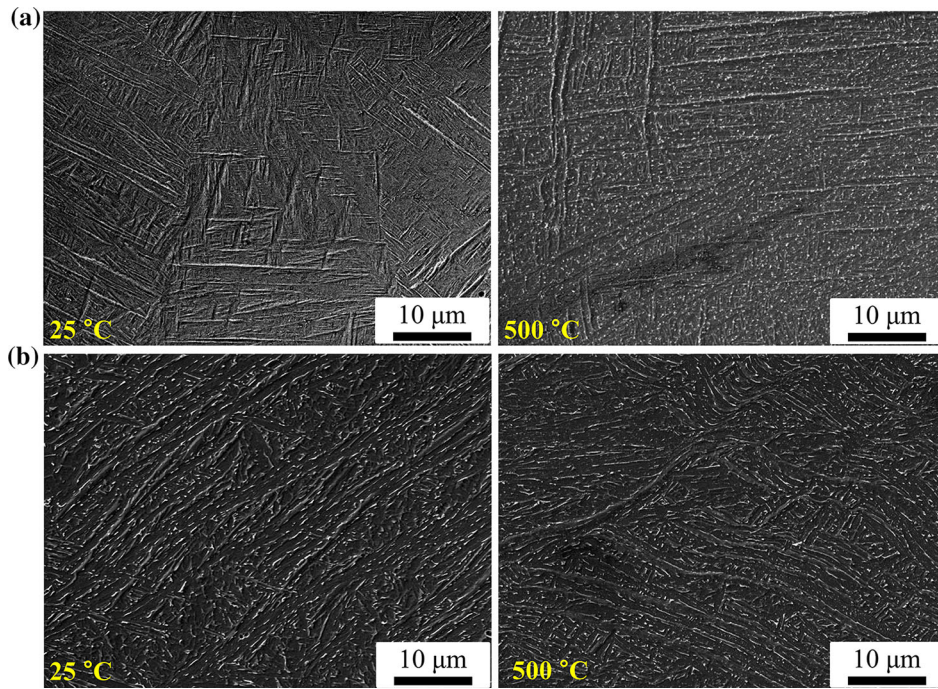
Fig. 11—Microstructures after compressive deformation of SLM Ti64 alloys at 25 °C and 500 °C: (*a*) as-fabricated specimen and (*b*) heat-treated specimen.
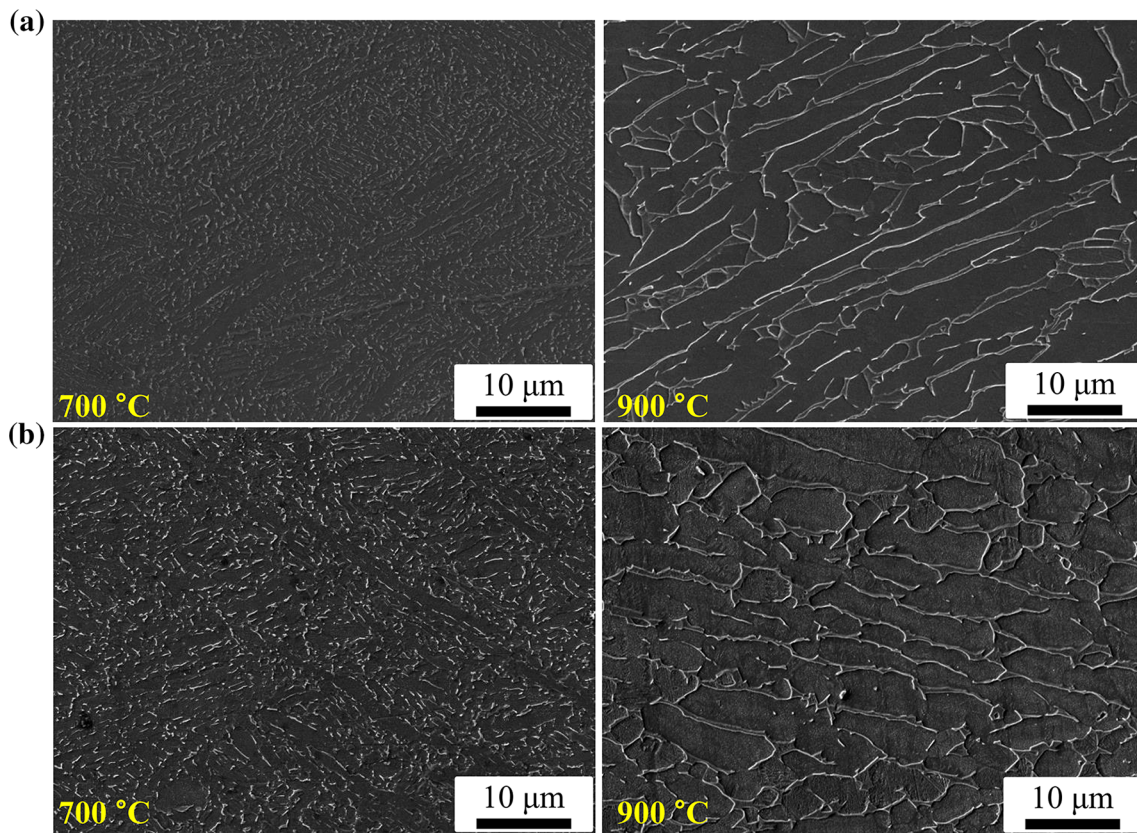

Fig. 12—Microstructures after compressive deformation of SLM Ti64 alloy at 700 °C and 900 °C: (*a*) as-fabricated specimen and (*b*) heat-treated specimen.

properties is expected to have disappeared due to DRX. Deformed microstructure before and after the heat treatment specimen tested at 700 °C showed nearly no martensite phases, unlike the room-temperature and 500 °C conditions, and a fine $\alpha + \beta$ lamellar structure was observed. In other words, martensite phase is completely decomposed through DRX and this is assumed to be the cause of the dislocation density decrease, which results in the decrease and elimination of mechanical property differences. In the 900 °C, compressively deformed microstructure, where yield strength is decreased further, a relatively coarse $\alpha + \beta$ lamellar structure compared to 700 °C was observed. More importantly, the as-fabricated and heat-treated specimens achieved excellent mechanical properties due to the formation of α'-martensite structure as a result of the fast cooling rate and the increase in dislocation density. Also, the martensite fraction was confirmed to be the source of differences in mechanical properties and deformation/fracture behavior between the two specimens; the microstructural evolution, such as DRX, at temperatures of 700 °C to 900 °C was also confirmed to cause similar behaviors.

IV. CONCLUSIONS

This study investigated and analyzed the influence of stress relieving heat treatment (650 °C, 3 hours) on microstructure and room- and high-temperature compressive properties of Ti64 alloy manufactured by SLM. The following are the main conclusions.

1. Initial microstructural observation confirmed that prior β grain elongated in the direction where heat is discharged and acicular type α'-martensite structures were formed within the β grain. Also, XRD and misorientation angle distribution analysis confirmed that phase decomposition of some α' and dislocation density decreased after stress relieving heat treatment
2. Room-temperature hardness anisotropy appeared in the as-fabricated specimen; on the other hand, the average hardness decreased by 10 pct, and at the same time, the hardness anisotropy disappeared in the heat-treated specimen. Room- and high-temperature compression tests confirmed that the room-temperature yield strength was approximately 1365 MPa for the as-fabricated specimen and 1138 MPa for the heat-treated specimen, which is similar to or greater than those of wrought materials. The as-fabricated specimen had greater yield strength than the heat-treated specimen up to the 500 °C condition, but at temperatures of 700 °C or higher, both specimens showed a drastic strength decrease and differences in mechanical properties disappeared.
3. Surface observation after the room-temperature compression test confirmed that the as-fabricated specimen failed to accommodate most of the deformation, resulting in fractures, while the heat-treated specimen accommodated most of the deformation. At temperatures of 500 °C or higher, both specimens showed ductile characteristics where fractures or shear cracks were not formed. Meanwhile, for room-temperature to 500 °C compression specimens, which did have differences in mechanical properties, the microstructure after the compression test was similar to that of the initial microstructure. The martensite structure was completely decomposed in the case of the specimens compressed at temperatures of 700 °C or higher with similar mechanical properties

REFERENCES

1. M. Vaezi, H. Seitz, and S. Yang: *Int. J. Adv. Manuf. Technol.*, 2013, vol. 67, pp. 1721–54.
2. L. Facchini, E. Magalini, and P. Robotti: *Rapid Prototyp. J.*, 2009, vol. 15, pp. 171–78.
3. C. Qiu, N.J.E. Adkins, and M.M. Attallah: *Mater. Sci. Eng. A*, 2013, vol. 578, pp. 230–39.
4. E.J. Bae, J.H. Kim, W.C. Kim, and H.Y. Kim: *J. Adv. Prosthodont.*, 2014, vol. 6, pp. 266–71.
5. B. Nie, H. Huang, S. Bai, and J. Liu: *Appl. Phys. A*, 2015, vol. 118, pp. 37–41.
6. S. Bremen, W. Meiners, and A. Diatlov: *Laser Tech. J.*, 2012, vol. 9, pp. 33–38.
7. F. Abe, K. Osakada, M. Shiomi, K. Uematsu, and M. Matsumoto: *J. Mater. Process. Technol.*, 2001, vol. 111, pp. 210–13.
8. Z. Lijing, L. Yingying, S. Shaobo, and Z. Hu: *Chin. J. Aeronaut.*, 2015, vol. 28, pp. 564–69.
9. D. Gu, Y.C. Hagedorn, W. Meiners, G. Meng, RJS. Batista, K. Wissenbach, and R. Poprawe: *Acta Mater.*, 2012, vol. 60, pp. 3849–60.
10. M. Simonelli, Y.Y. Tse, and C. Tuck: *Annual International Solid Freeform Fabrication Symposium*, University of Texas, Austin, TX, 2012.
11. R.A. Wood: *Titanium Alloy Handbook*, Metals and Ceramics Information Center, Battelle, Columbus, OH, Dec 1972, publication no. MCIC-HB-02.
12. J.P. Blanchard, A. Chen, and B. Qiu: *Nucl. Instrum. Meth. B*, 1993, vol. 82, pp. 63–68.
13. M.K. Mcquillan: *J. Metall. Rev.*, 1963, vol. 8, pp. 41–104.
14. M. Niinomi: *Mater. Sci. Eng. A*, 1998, vol. 243, pp. 231–36.
15. I. Gurrappa: *Mater. Charact.*, 2003, vol. 51, pp. 131–39.
16. F.H. Froes, H. Friedrich, J. Kiese, and D. Bergoint: *JOM*, 2004, vol. 56, pp. 40–44.
17. Q. Huang, X. Liu, X. Yang, R. Zhang, Z. Shen, and Q. Feng: *Front. Mater. Sci.*, 2015, vol. 9, pp. 373–81.
18. B. Vrancken, L. Thijs, JP. Kruth, and J.V. Humbeeck: *J. Alloy Compd.*, 2012, vol. 541, pp. 177–85.
19. G.M.T. Haar and T.H. Becker: *Materials*, 2018, vol. 11(1), p. 146.
20. H.K. Rafi, T.L. Starr, and B.E. Stucker: *Int. J. Adv. Manuf. Technol.*, 2013, vol. 69, pp. 1299–1309.
21. T. Vilaro, C. Colin, and J.D. Bartout: *Metall. Mater. Trans. A*, 2011, vol. 42A, pp. 3190–99.
22. S. Leuders, M. Thone, A. Riemer, T. Niendorf, T. Troster, H.A. Richard, and H.J. Maier: *Int. J. Fatigue*, 2013, vol. 48, pp. 300–07.
23. Y.K. Kim, S.H. Park, J.H. Yu, B. AlMangour, and K.A. Lee: *Mater. Sci. Eng. A*, 2018, vol. 715, pp. 33–40.
24. B. Baufeld, O.V.D. Biest, and R. Gault: *Mater. Des.*, 2010, vol. 31, pp. S106–S111.

25. S.L. Campanelli, N. Contuzzi, A.D. Ludovico, F. Caiazzo, F. Cardaropoli, and V. Sergi: *Materials*, 2014, vol. 7, pp. 4803–22.
26. T. Becker, M.V. Rooyen, and D. Dimitrov: *S. Afr. J. Ind. Eng.*, 2015, vol. 26, pp. 93–103.
27. M. Simonelli, Y.Y. Tse, and C. Tuck: *Metall. Mater. Trans. A*, 2014, vol. 45A, pp. 2863–72.
28. T.J. Ruggles, T.M. Rampton, A. Khosravani, and D.T. Fullwood: *Ultramicroscopy*, 2016, vol. 164, pp. 1–10.
29. M. Calcagnotto, D. Ponge, E. Demir, and D. Raabe: *Mater. Sci. Eng. A*, 2010, vol. 527, pp. 2738–46.
30. S.H. Joo, H. Kato, M.J. Jang, J. Moon, C.W. Tsai, J.W. Yeh, and H.S. Kim: *Mater. Sci. Eng. A*, 2017, vol. 689, pp. 122–33.
31. L. Thijs, F. Verhaeghe, T. Craeghs, J.V. Humbeeck, and J.P. Kruth: *Acta Mater.*, 2010, vol. 58, pp. 3303–12.
32. LE. Murr, E.V. Esquivel, S.A. Quniones, S.M. Gaytan, M.I. Lopez, E.Y. Martinez, F. Medina, D.H. Hernadez, E. Martinez, J.L. Martinez, S.W. Stafford, D.K. Brown, T. Hoppe, W. Meyers, U. Lindhe, and R.B. Wicker: *Mater. Charact.*, 2009, vol. 60, pp. 96–105.
33. B. Vandenbroucke and J.P. Kruth: *Rapid Prototyp. J.*, 2007, vol. 13, pp. 193–203.
34. L. Facchini, E. Magalini, P. Robotti, A. Molinari, S. Hoges, and K. Wissenbach: *Rap. Prototyp. J.*, 2010, vol. 16, pp. 450–59.
35. M. Vanderhasten, L. Rabet, and B. Verlinden: *Metalurgija*, 2005, vol. 11, pp. 195–200.
36. J.A. Hines and K.S. Vecchio: *Acta Mater.*, 1997, vol. 45, pp. 635–49.